Mobile Integrons Encode Phage Defence Systems

Nicolas KIEFFER[1,2♦], Alberto HIPÓLITO[1,2♦], Paula BLANCO[1,2], Thomas DELOBELLE[3], Laura ORTIZ-MIRAVALLES, Francisco Manuel OJEDA[1,2], Thomas JOVÉ[4], Dukas JURENAS[3], Meritxell GARCÍA-QUINTANILLA[5,6], Pilar DOMINGO-CALAP[7], José Antonio ESCUDERO[1,2*]

[1]Molecular basis of Adaptation Laboratory, Departamento de Sanidad Animal, Facultad de Veterinaria de la Universidad Complutense de Madrid, Madrid, España,
[2]VISAVET Health Surveillance Centre, Universidad Complutense de Madrid, Spain.
[3] Laboratoire de Génétique et Physiologie Bactérienne, Faculté de Sciences, Université Libre de Bruxelles (ULB), Gosselies, Belgium.
[4]INSERM, CHU Limoges, RESINFIT, University of Limoges, Limoges, France, Present address: no longer employed by INSERM.
[5]Departamento de Microbiología, Instituto de Investigación Sanitaria Fundación Jiménez Díaz, Madrid, España
[6]CIBERINFEC-CIBER de Enfermedades Infecciosas, Instituto de Salud Carlos III, Madrid, Spain
[7]Instituto de Biología Integrativa de Sistemas, Universitat de València-CSIC, Paterna, Spain.

♦Both authors contributed equally

*Corresponding Author. Email: jaescude@ucm.es
+34 661584761
University Complutense of Madrid,
Department of Animal Health,
Avenida Puerta de Hierro s/n
28040, Madrid, Spain.

ABSTRACT

Integrons are bacterial genetic elements that capture, stockpile and modulate the expression of genes encoded in integron cassettes. Mobile Integrons (MI) are borne on plasmids, acting as a vehicle for hundreds of antimicrobial resistance genes among key pathogens. These elements also carry gene cassettes of unknown function (*gcu*s) whose role and adaptive value remains unexplored. Recent years have witnessed the discovery of a myriad defence systems against bacteriophages, highlighting that viral infection is a major selective pressure for bacteria. We hence sought to explore if *gcu*s could encode phage defence systems. Using the INTEGRALL database, we established a collection of 129 *gcu*s in pMBA, a vector where cassettes are established as part of a class 1 integron. PADLOC and DefenseFinder predicted four phage defence systems in this collection, comprising Lamassu, CBASS and two ABI (abortive infection) systems. We experimentally challenged all cassettes with phages and found nine additional candidates that were not detected *in silico*. We have characterized in depth the 13 *gcu*s against a panel of phages in *Escherichia coli* confirming their role as phage defence integron cassettes (PICs). We used recombination assays to verify that all systems are *bona fide* integron cassettes and are therefore mobile. We show that PICs confer resistance in other clinically relevant species, such as *Klebsiella pneumoniae* and *Pseudomonas aeruginosa.* Several PICs also limit prophage activation, providing protection at the population-level. Given the stockpiling capacity of integrons, we explored the additivity of phenotypes and found that integrons with two PICs confer multiphage-resistance. Additionally, when combined with antimicrobial resistance genes, integrons confer simultaneously drug and phage resistance. Crucially, we also show that the position of a *pic* in the array can strongly decrease its cost. Our results prove a role of integrons in phage defence, acting as highly mobile, low-cost defence islands. This has important implications in the spread of defence systems, and on the future of phage therapy.

62 **INTRODUCTION**

63 Antimicrobial resistance (AMR) is a major public health concern worldwide, and the
64 emergence of multi-drug (MDR) resistant bacteria is making increasingly difficult to treat
65 infections with antibiotics[1]. Alternative therapeutic options are being explored as potential
66 solutions to this problem. Phage therapy -the use of viruses that infect and kill bacteria- is an
67 old approach (it predates the use of antibiotics) that is currently being revisited and building
68 momentum. Several recent reports have yielded positive results for the treatment of life-
69 threatening infections caused by MDR bacteria[2–4]. However, the efficacy of phage therapy can
70 be limited by the emergence of phage-resistant bacteria[5,6]. Resistance can typically emerge
71 through mutations in which the receptors recognized by the phage are lost, or through the
72 acquisition of defence systems. In recent years, a plethora of new defence systems have been
73 discovered and characterized to varying extents, adding to the classic restriction-modification
74 enzymes or the more modern CRISPR-Cas immune systems[7]. These can be classified according
75 to the mechanism used to sense phage infection into systems that detect nucleic acids, phage
76 proteins, the integrity of the host, and others[8,9]. These defence mechanisms have evolved in
77 response to phage predation, and they are often encoded in the vicinity of other systems,
78 creating defence islands. In fact, it was the proximity to known defence systems that allowed
79 the initial discovery of systems such as Lammasu, Kiwa, Thoeris, or Zorya, using a guilt-by-
80 association rationale[9–11]. Ever since, we have witnessed a sheer increase in the discovery of
81 novel defence systems. Their abundance in genomes illustrates the ongoing evolutionary arms
82 race between bacteria and their phages and highlights the importance of phage predation as a
83 selective pressure for bacteria[12]. Defence systems have been shown to be encoded in mobile
84 genetic elements such as integrative conjugative elements, transposons, or prophages[12].
85 However, they are proven to impact the fitness of the bacterial strains carrying them due to the
86 constitutive expression of their genetic content[13] highlighting the cost of resistance.

87 Integrons are genetic elements that play an important role in bacterial adaptation to
88 changing environmental conditions[14–16]. They capture and accumulate new genes embedded in
89 integron cassettes (ICs), acting as genetic memories of adaptive functions[17]. Integrons typically
90 consist of a conserved platform encoding the integrase gene and the recombination site in the
91 integron (*attI*)[18]; and a variable region containing the cassettes. Cassettes are incorporated into
92 the *attI* site through site-specific recombination reactions mediated by the integrase and are
93 expressed from the dedicated Pc promoter encoded in the platform[19]. The integrase can also
94 reorder cassettes in the array to modulate their expression, modifying their distance to the Pc

and the polar effects they are subjected to[20–22]. The expression of the integrase is controlled by the SOS response, so that integrons provide to their hosts "adaptation on demand"[23,24].

Mobile integrons (MI) are a subset of integrons that are typically associated with mobile genetic elements, such as plasmids and transposons, which can facilitate their horizontal transfer between bacterial cells[25–27]. They are a palpable example of the evolvability these platforms confer to their hosts. They were initially discovered in the first MDR isolates of *Shigella* spp. during the 1950's, carrying two resistance genes[16,28]. Nowadays MIs are commonplace among key Gram-negative pathogens[29] carrying almost 200 resistance genes against most antibiotic families[30–32]. Consequently, MIs are generally considered to be devoted almost exclusively to AMR. Nevertheless, among the cassettes found within MIs are gene cassettes of unknown function (*gcu*) whose importance has generally been overlooked. Yet the working model of integrons suggests that cassettes must be adaptive at the time of integration when they are expressed at the maximum strength[23]. We hence reasoned that *gcu*s could be playing an unknown adaptive role. Given the importance of phage predation in the lifestyle of bacteria and in their genome's content, we sought to explore the possibility that *gcus* encode phage defence systems.

Here we have selected 129 *gcus* from the INTEGRALL database[33], and cloned them in pMBA, a plasmid mimicking the genetic environment of a mobile integron[32]. DefenseFinder[34] and PADLOC[35] predicted 4 *gcus* in the collection as potential defence systems. We then used *in vitro* screening test using phages T4 and T7 combined with structural prediction using AlphaFold and discovered 9 novel defence systems that were not predicted. All cassettes confer resistance to at least one of a panel of 8 phages against *E. coli*. We have confirmed that all systems are encoded in *bona fide* (functional) integron cassettes, which we have named Phage defence Integron Cassettes (PICs), and are hence mobile and likely to circulate among other species. Indeed, we demonstrate that they also confer resistance in *K. pneumoniae* and *P. aeruginosa,* major pathogens of the ESKAPEE group. As part of an integron, cassettes can be stockpiled in an array. Building arrays we show that phenotypes of PICs are additive, conferring multi-phage or phage/drug resistance if combined with other PICs or antimicrobial resistance cassettes (ARCs). We also show that the position of a PIC in the array can strongly diminish its cost. Altogether, our work proves the involvement of integrons in phage defence, acting as repositories of a broad variety of defence systems i.e.: as mobile and low-cost defence islands.

129 **RESULTS**

130 **Integron *gcus* contain predicted phage defence systems.**

131 To obtain a broad set of *gcu*s in MIs we screened the INTEGRALL database, the largest
132 repository for mobile integron-related data (date: November 2021). We retrieved 303 cassettes
133 annotated as *gcu*s (< 95% nucleotide identity) with sizes ranging from 191 bp to 3 kb. We
134 further analysed and curated this list manually using BLAST. We discarded several cassettes
135 misannotated as *gcu*s in which an insertion sequence had interrupted a cassette of known
136 function. Additionally, gene-less cassettes -that failed to produce hits with any known or
137 unknown protein- were also discarded. We therefore selected a panel of 129 elements with sizes
138 ranging from 284 to 2.950 bp (Figure S1). All elements were synthesized *in vitro* and cloned in
139 pMBA, a vector providing a biologically sound genetic environment, where cassettes are
140 inserted in first position of a class 1 integron and are under the control of a strong Pc promoter
141 (PcS)[32]. The sequences of our selected collection were submitted in May 2022 to the two major
142 web platforms specialized in phage resistance gene prediction, DefenseFinder and
143 PADLOC[34,36]. As a result of this computational analysis, we identified four distinct gene
144 cassettes (*gcu*s 59, 128, 135 and N) as potential defence mechanisms, each exhibiting homology
145 to a known system involved in phage resistance (Figure 1A).

146 Given their newly identified putative function as phage resistance elements, we propose
147 to rename these *gcus* as *pic*s, while conserving their initial name for simplicity. Pic59 (formerly
148 Gcu59) was identified as a homolog of the AriAB system[37] and is suggested to confer phage
149 resistance through abortive infection. *pic128* encodes two ORFs (*pic128A* and *pic128B*) and
150 shows similarity to a Lamassu Type 1 system. AlphaFold predicts that Pic128A shares motifs
151 with YfjL-like or AbpA proteins, which are involved in phage defence, while Pic128B contains
152 a putative exonuclease domain. Interestingly, the three-dimensional structure of Pic128B
153 protein displays a remarkable similarity to DdmC, a protein from the Lamassu Type 2 plasmid
154 and phage defence system described in *Vibrio cholerae*[38]. *pic135* also contains two ORFs and
155 share structural similarity with a CBASS Type 1 system[39]. The proteins encoded by this cassette,
156 Pic135A and Pic135B, are predicted to play roles in nucleotidyl-transfer and membrane
157 translocation, respectively, as suggested by protein structure predictions. Last, PicN is
158 annotated as an AbiV family protein[40], implicated in phage resistance through abortive infection
159 mechanisms.

160

161

162

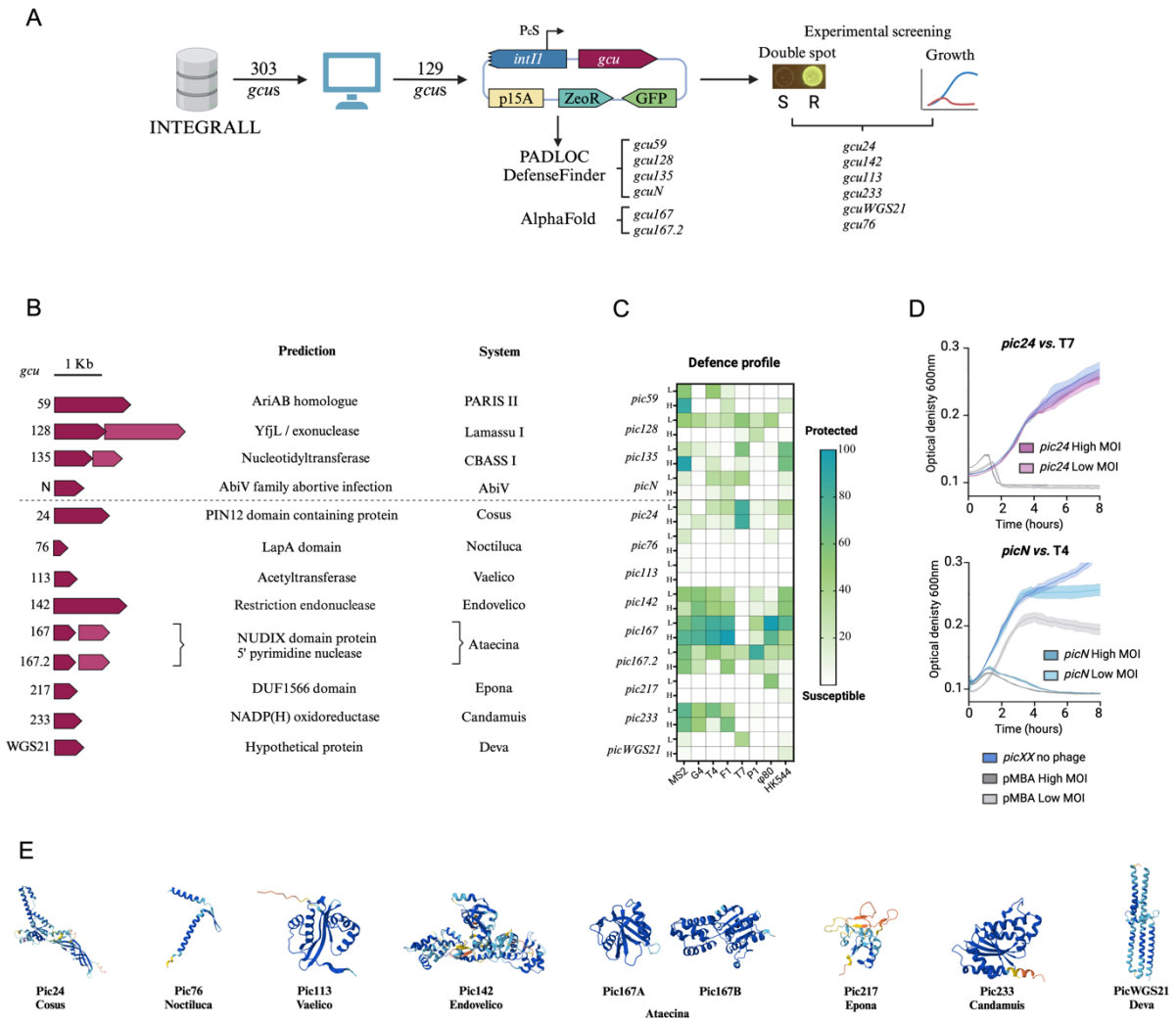

Figure 1. Identification and Characterization of Phage Defense Systems in Integron Cassettes. (A) Schematic workflow for the identification and experimental validation of phage defence systems in *gcus*. A collection of 303 gcus was extracted from the INTEGRALL database, curated to 129 *gcus*, and cloned into the pMBA vector, placing each *gcu* under the control of a strong integron promoter (PcS). Predicted phage defence systems were identified using PADLOC and DefenseFinder, (May 2022) and experimental screening was performed using a double-spot assay or growth curves to determine susceptibility or resistance to phage infection. **(B)** Genetic organization and predicted functions of selected *gcus*. Predicted function is shown for putative defence mechanisms and other candidate *gcus*. **(C)** Heatmap showing the defence profiles of identified Phage Integron Cassettes (PICs) against a panel of eight *E. coli* phages. The degree of protection (resistance) is indicated by the color scale, with dark green representing high protection, light green representing low protection, and white no protection. **(D)** Examples of growth curves used to build the heatmap in C: *pic24* confers strong resistance to phage T7 at both high and low MOI while *picN* shows resistance to phage T4 only at low MOI. Growth curves are represented as the mean of three independent replicates. The standard error of the mean is represented as a lighter colour shade. **(E)** Structure of novel phage defence systems, as predicted by AlphaFold2.

Functional screening and domain prediction reveal additional phage defence systems.

Bioinformatic approaches can fail to detect novel systems that are not similar to any of the known ones. We hence turned to *in vitro* experiments to detect novel resistance mechanisms within our *gcu* collection. We employed a double spot screening protocol in solid media and the monitoring of growth curves in liquid media, to challenge the whole collection with different

181 concentrations of phages T4 or T7 (Figure 1A and Figure S2). We successfully detected 7 new
182 candidates (*pic24, pic142*, *pic233, pic217, pic113, picWGS21* and *pic76*) presenting substantial
183 growth in the presence of phage (Figure S2). Using AlphaFold prediction model to find proteins
184 with potential nuclease domains, that are often linked to phage defence, we additionally
185 identified *pic167* and its close homolog *pic167.2*. *in silico* structural predictions of proteins
186 encoded in these PICs suggest a diversity of functional roles. Both Pic167 and Pic167.2 are
187 likely involved in nucleotide metabolism, with indications of NUDIX hydrolase and
188 nucleotidase activities. Pic142 is a putative restriction endonuclease, while Pic24 possesses a
189 PIN12 domain that potentially acts as a nuclease[41]. Pic233 is possibly a NADP(H)
190 oxidoreductase; Pic113 is a putative GNAT N-acetyltransferase and Pic217 a putative integral
191 membrane protein with a lectin C domain. AlphaFold did yield relevant homologs with a known
192 function for PicWGS21. Last, Pic76 is a small protein of 76 amino acid that contains a LapA
193 domain that has been related to biofilm formation[42] (Figure 1B). To adhere to the custom in the
194 field, these novel systems are also given the name of a deity of Celtiberian mythology (Figure
195 1B).
196
197 **PICs confer protection to a panel of phages *Escherichia coli.***
198 To characterize in depth the role and profile of PICs in phage resistance, we subcloned
199 the whole library in strain *E. coli* IJ1862 (an F' strain that can be infected by plasmids targeting
200 the conjugative pilus[43]) and conducted infection assays with a panel of phages from different
201 families at varying multiplicities of infection (MOIs). We monitored the optical densities
202 (OD_{600}) over time of bacterial cultures in presence and absence of phage MS2, F1, G4, T4, T7,
203 P1, Φ80 and HK544. As a control, we included an isogenic strain carrying the empty vector
204 pMBA. We used the area under the (growth) curve to determine the protective effect of the
205 cassette, as in[44] (see Materials and Methods). Our data showed that all PICs conferred resistance
206 to at least one condition (one phage at one MOI) (Figure 1C and Figure S3), confirming their
207 role in phage defence. Resistance profiles were diverse, with some PICs showing broad-
208 spectrum resistance, such as *pic167, pic167.2*, *pic128* and *pic142*. Others, as *pic24,* showed a
209 narrower spectrum with low level resistance against several phages, but very high resistance
210 against phage T7 at both high and low MOI (Figure 1D). The resistance phenotype displayed
211 by *picN*, limited to low MOI for phages MS2, T4, F1 and T7, aligns with the characteristic
212 phenotype of an abortive infection, thereby confirming the predictions made by PADLOC and
213 DefenseFinder. Overall, our results confirm that the *gcus* identified in our screenings are indeed
214 phage resistance genes with known and characterized mechanisms.

215

216 **PICs are *bona fide* integron cassettes.**

217 Identification of integrons and their cassettes has not been a straightforward task until
218 the appearance of IntegronFinder[45]. A large part of the content in INTEGRALL predates
219 IntegronFinder, so their classification as integron cassettes needs to be verified. A close analysis
220 of the genetic context, locating integrases in close vicinity and in opposite orientation, can be
221 indirect proof that a gene is indeed a cassette. Most PICs identified here -except for *pic135* and
222 *pic142*- are located within class 1 or class 2 integrons, often in pathogenic strains belonging to
223 the *Enterobacteriaceae* family (like *pic217*, *pic113*, and *pic24*) or multidrug resistant *P.*
224 *aeruginosa.* A compelling example of the latter is the presence of *picN* next to cassettes $bla_{IMP,}$
225 *aacA4* and *catB6,* conferring multidrug resistance to carbapenems, aminoglycosides, and
226 chloramphenicol, respectively (Accession number: AJ223604) (Figure 2A). Yet, given that
227 finding defence systems in integrons has important implications for the mobility of these
228 systems, we sought to verify experimentally that these are *bona fide* integron cassettes. Cassette
229 recombination is a site-specific reaction that can be evidenced in a suicide conjugation assay
230 that is typical in the field[16,46]. Crucially, recombination is semiconservative, involving the
231 bottom strand (but not the top strand) of both the *attC* sites in cassettes and *attI* sites of integrons
232 [47,48]. This unique feature can be easily detected because it leads to clear differences in the suicide
233 conjugation assay when the plasmid transfers the bottom or top strand of the cassette[48]. With
234 this in mind, we inserted the putative *attC* sites of all *pics* in both orientations in the suicide
235 vector pSW23T and measured the recombination frequency of both strands for each cassette.
236 Recombination events were verified through PCR. As expected, we observed a clear drop
237 (between 100- and 10.000-fold lower) in the recombination frequency of the top strands of all
238 putative *attC* sites, as would be expected from integron cassettes (Figure 2B). *picWGS21* had
239 extremely low recombination frequencies for the bottom strand. Yet recombination of the top
240 strand was only observed in 1 out of 6 replicate experiments, suggesting that it is indeed an
241 integron cassette albeit with a very poor recombination site. Indeed, the folded *attC* site of
242 *picWGS21* has the typical hairpin structure and extra-helical bases of these sites (Figure S4)[48–
243 50]. Hence, our data confirms that PICs are *bona fide* integron cassettes.

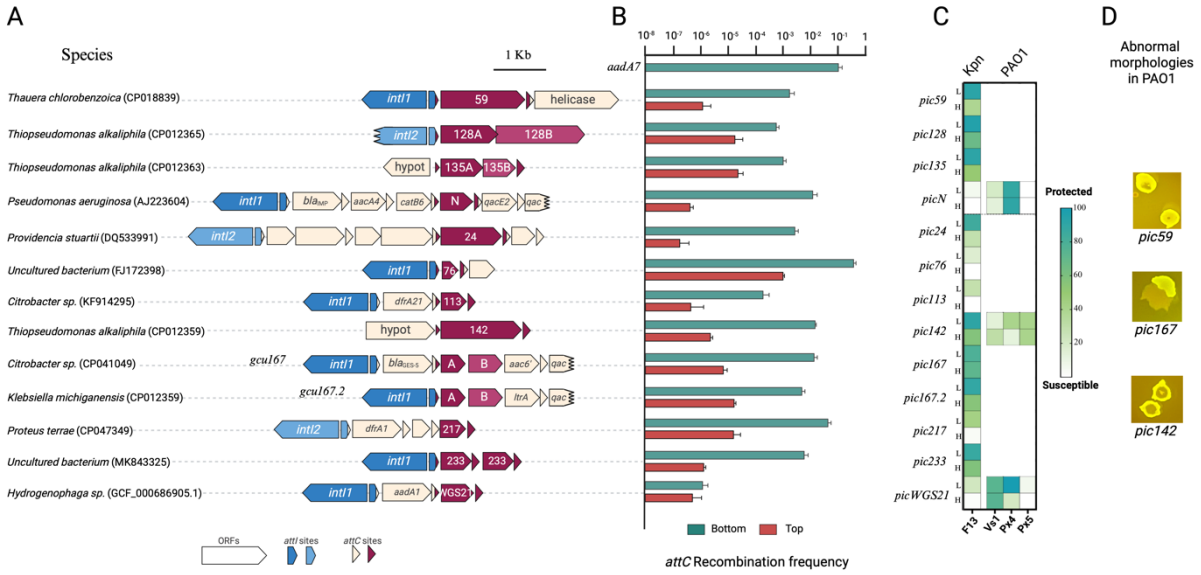

Figure 2. Genetic Context, Recombination Frequency, and Phage Protection Profiles of Identified PICs in other species. (A) Genetic context of PICs as found in databases, highlighting their association with integron integrases (*intI1* or *intI2*, in blue shades). PICs are found in different host species. Each PIC is annotated with its respective identifier (e.g., 59, 128A/B, 135A/B), along with known associated genes such as resistance genes (e.g., bla_{IMP}, *aacA4*, *catB6*). **(B)** Recombination frequency of the *attC* sites of the identified PICs. The recombination frequency was measured for the bottom (green bars) and top (red bars) strands of the *attC* sites using a suicide conjugation assay. Bars represent the mean of at least 3 biological replicates. Error bars correspond to the standard error of the mean. **(C)** Heatmap showing the protection profiles of PICs against phage infection in different host species, including *K. pneumoniae* (Kp5) and *P. aeruginosa* (PAO1) against a panel of cognate phages (F13, Vs1, Px4, Px5).

Defence cassettes are protective in other species.

Given the mobility of integrons and cassettes among important pathogens, we sought to determine if PICs are active in different hosts. To this end, we evaluated the protective effects of PICs in *K. pneumoniae* and *P. aeruginosa,* two species of the ESKAPEE group of highly resistant and lethal pathogens where integrons are prevalent. We introduced all PICs into *K. pneumoniae* Kp5, a MDR clinical isolate. We sequenced the genome of this strain and found three plasmids, one of which contains a class 1 integron (full resistome can be found in Table S1). The PHASTEST software did not detect prophages in the genome of Kp5. We subjected all strains to infection with the *Drexlerviridae* phage F13 co-isolated with the strain. All PICs, except *picN*, demonstrated resistance to F13 at low MOI. Most of them also conferred resistance at high MOI (except *pic76*, *pic113*, *pic217*, and *picWGS21*) (Figure 2C). To introduce PICs in *P. aeruginosa* PAO1 strain, we changed the p15A origin of replication of pMBA for BBR1, and introduced a tetracycline resistance marker. After several assays, we could only transform *picN* successfully, while other PICs produced no colonies at all or abnormal (sick) colony morphologies (Figure 2D). This led us to hypothesize that some *pics* might be toxic or extremely costly in this background. To avoid this, we changed the strong promoter guiding the

270 expression of cassettes in pMBA (PcS) for a weaker version (PcW). This way we could
271 introduce *pic24, pic113, pic142* and *picWGS21* in PAO1 and were able to measure their
272 activities. We confronted these strains to a collection of 36 phages infecting PAO1 using a
273 double spot screen. We observed growth for *picN*, *pic142* and *picWGS21* in presence of phages
274 Vs1, Px4 and Px5. We evaluated the level of resistance by monitoring growth curves for each
275 PIC against the three phages, and confirmed their resistance phenotype (Figure 2C). *pic142* -
276 that had a clear phenotype against several phages both in *E. coli* and *K. pneumoniae*- confirmed
277 its broad spectrum and host range, conferring resistance to Px5 at both MOI and to Px4 at low
278 MOI ; contrarily, *picN* and *picWGS21,* that had only showed low resistance against a handful
279 of phages in *E. coli*, conferred very high resistance against phage Px4 and Vs1 in *P. aeruginosa*.
280 Altogether, our data proves that PICs can confer resistance to different phages and in different
281 host species. Although some PICs seem to have a defined narrow host range, others, like *pic142*
282 were able to confer resistance in the three species against most phages tested, underlying the
283 broad-spectrum activity of this defence mechanism.
284
285 **PICs protect against prophage activation.**
286 An important aspect of the interplay between phages, their hosts, mobile genetic
287 elements and defence systems is the case of prophage activation. Hindering activation of
288 prophages can both protect at the cell and at the population level. Here we asked if a plasmid
289 carrying a mobile integron with a PIC can limit the production of phage particles from a
290 chromosomally encoded prophage once it switches to lytic cycle. To test this, we introduced all
291 PICs in lysogens of *E. coli* 594 with either HK544 or Φ80 prophages in their genomes. We
292 induced prophage activation with mitomycin and quantitated the phage titer after 6 hours.
293 *pic128*, *pic135* and *pic142* showed mild to strong defence against the activation of HK544, with
294 20 to 1.000 fold decreases in plaque forming units. Pic59 completely abolished the production
295 of HK544 virions, showing $>10^7$ fold protection (Figure 3A). Resistance against Φ80 activation
296 was generally low, with only *picN, pic167,* and *pic233* producing statistically significant
297 resistance levels. Interestingly, there is not a clear correlation between defence against the free
298 form of the phage (Figure 1C) and the activation of the prophage. Certain systems, like *pic135*
299 and *pic142* confer resistance against both forms of a phage (HK544); while others, like *pic128*,
300 *pic167*.2 and *pic217* only conferred resistance against one. These results show that mobile
301 integrons containing PICs can interfere with prophage activation, highlighting the potential
302 protective effect at the community level, and the complex interplay between mobile genetic
303 elements.

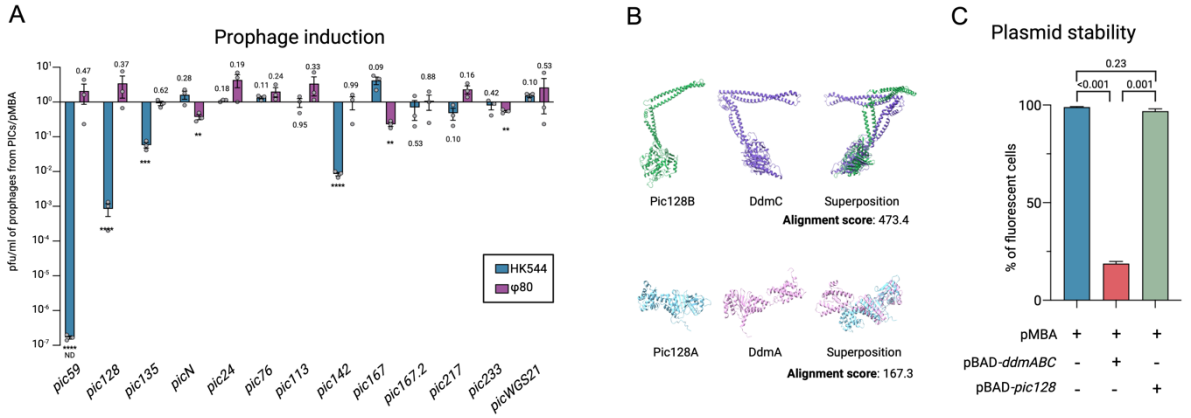

Figure 3. Prophage Induction, Structural Alignment, and Impact of *pic128* on Plasmid Stability. **(A)** Prophage induction assays inducing with mitomycin (0,5 µg/ml). The graph shows the concentration of phage (measured as plaque-forming units per millilitre (pfu/ml)) when activating prophages in the presence of pMBA containing PICs over the empty pMBA. ND: not detected (Limits of detection plotted). One sample *t* and Wilcoxon test; *P* values are shown when possible; ** < 0.01; *** < 0.001; ****<0.0001. **(B)** Structural alignment using FoldSeek of Pic128A and Pic128B proteins with known phage and plasmid defence proteins DdmA and DdmC, respectively. Superposition of protein structures is shown, with alignment scores indicating the degree of structural similarity. **(C)** Plasmid stability assays in *E. coli*. The percentage of fluorescent cells, representing the stability of pMBA, is shown for strains containing the pBAD plasmid with either the *ddmABC* or *pic128AB* systems. While *ddmABC* significantly reduces plasmid stability, *pic128* does not show a significant effect, indicating no anti-plasmid activity. Bars represent the mean of at least 3 biological replicates. Error bars correspond to the standard error of the mean. Statistical significance was assessed through unpaired t-tests and *P* values are shown.

pic128 does not have anti-plasmid activity.

DdmABC is a phage and plasmid defence system. It has been shown to confer phage resistance in *E. coli* and to cure plasmids in *Vibrio cholerae*, particularly those with a p15A replication origin[38]. When modelling protein structures of PICs, we found strong similarities between Pic128B and DdmC (Figure 3B), proteins that belong to (different) Lamassu defence systems. Interested by the interactions between mobile elements, we set out to examine whether the expression of *pic128AB* could exert a similar influence on plasmid stability. Because pMBA has a p15A replication origin, we decided to investigate the antiplasmid activity of *pic128AB* from a different vector. We hence cloned *pic128AB* and *ddmABC* systems into a pBAD plasmid that possess a pBR322 origin of replication and co-transformed them with an empty pMBA. We induced both systems with arabinose and monitored the loss of pMBA as the presence of non-fluorescent colonies for 3 days (ca. 20 generations). pMBA is stably maintained in the absence of antibiotics, with 99% of the cells in the population being fluorescent after 3 days. As expected, DdmABC strongly decreased the proportion of fluorescent colonies to 19% by day 3 (Figure 3C), while pMBA was stably maintained at >97% in the presence Pic128AB. This suggests that, despite their structural similarities, Pic128AB does not have the anti-plasmid activity detected for DdmABC. Still, both systems could have different plasmid specificities,

334 so we extended our plasmid stability studies to Kp5, carrying the three distinct natural plasmids
335 conferring resistance to tetracycline, ertapenem and cefotaxime, respectively. After introducing
336 pMBA-*pic128* into this isolate we assessed plasmid stability monitoring the loss of three
337 resistance phenotypes conferred by these replicons over a five-day period (Figure S5). We could
338 not observe a significant plasmid loss in any case, suggesting that *pic128* is not an anti-plasmid
339 system.
340
341 **Mobile Integrons can accumulate resistance to phages and antibiotics.**
342 The fact that integrons carry defence systems is important in the ecology and biology of
343 these systems. Integron cassettes can be stockpiled, and their phenotypes can be additive, as for
344 we have observed for multi-drug resistance MIs. It is hence possible that integrons can combine
345 PICs to provide multi-phage resistance; or PICs and antimicrobial resistance cassettes (ARCs)
346 providing phage- and AMR. This is important for phage therapy, since integrons would likely
347 play again -as it occurred with antibiotics- a key role in the evolution of resistance. Hence, we
348 sought to test if phage defence phenotypes can be additive and combined with antimicrobial
349 resistance genes. To do so, we first constructed pArray-1 an integron combining *pic24* ($T7^R$)
350 and bla_{OXA-10}, a class D β-lactamase gene that confers resistance to carbenicillin. The strain
351 carrying pArray-1 showed high levels of resistance against T7 and carbenicillin both separately
352 and simultaneously (Figure 4A). We then constructed pArray-2 containing *pic24* and *pic167.2*
353 (Figure 4A) that confer high and intermediate resistance to phage T7 and P1, respectively.
354 Strains carrying pArray-1 showed high resistance against both T7 and P1, highlighting the
355 additivity of phage resistance phenotypes. Our results show that, as predicted by the integron
356 model, integrons can combine phage resistance with AMR. Because MIs are enriched in AMR
357 genes, we can find several natural examples of the former among our PICs, with *picN*, *pic113*,
358 *pic167*, *pic217* and *picWGS21* located in integrons containing resistance genes against beta-
359 lactams, aminoglycosides, chloramphenicol and trimethoprim (Figure 2A). Because *gcus* are
360 less abundant, we did not find co-occurrence of pics within an array. Nevertheless, having
361 described a variety of two gene PICs, the genetic environment of *pic24* caught our attention and
362 was re-evaluated. This PIC is in a class 2 integron, preceded by two cassettes containing two
363 ORFs each. A new search with an updated version of DefenseFinder (June 2024) found
364 homologs of sensor protein ThsB from the Thoeris system in both cassettes (*gcu23* and *gcu24*).
365 It also found a type II restriction modification system downstream the last cassette of the
366 integron (Figure 4C). Both cassettes were in our initial collection but were not selected in our
367 screenings. In the case of *gcu23* we had not observed resistance in any case, while *gcu24* was

368 discarded because it yielded inconsistent results. We investigated this in more depth and
369 sequenced a variety of colonies from our *gcu24* stock. This revealed that the frequent
370 interruption of the cassette by the insertion of IS1, which explained the inconsistent results in
371 our screenings. We interpreted this as a sign of high fitness cost, so to test both cassettes we
372 cloned them in a modified pMBA under the control of a weak Pc promoter (PcW) (30-fold less
373 active than the PcS[51]) and tested them against the panel of phages in *E. coli* and *K. pneumoniae*.
374 *gcu22* conferred medium resistance exclusively against phage F13 in *K. pneumoniae*, while
375 *gcu23* had a broader defence profile, including very high resistance levels against G4, MS2, F1
376 and T4. We hence redefined them as PICs (*pic22* and *pic23*). Both cassettes share 50% bp
377 identity, and the ORFs share 17 and 37% identity in amino acid sequence respectively.
378 Nevertheless, the structure of the proteins in both systems is remarkably conserved. Despite the
379 homology of Pic22A and Pic23A with ThsB from Thoeris, Pic22B and Pic23B are not homologs
380 of ThsA and are located downstream, instead of upstream within the system. The structure of
381 these proteins is instead similar to that of the Deva system (*picWGS21*) (Figure 1E). Given this
382 apparent mix of systems, we called this system Tragantía (a deity with the upper body of a
383 woman and the lower body of a snake). We sought to prove that these natural arrangement of
384 cassettes act as a defence island. Given that only the phenotypes of *pic23* and *pic24* are
385 distinguishable, we built pArray-3 with *pic23* and *pic24* under the control of a PcW and showed
386 that it conferred multi-phage resistance (Figure 4C). Our data confirms that mobile integrons
387 act as mobile defence islands that are already circulating among livestock clinical isolates[52].

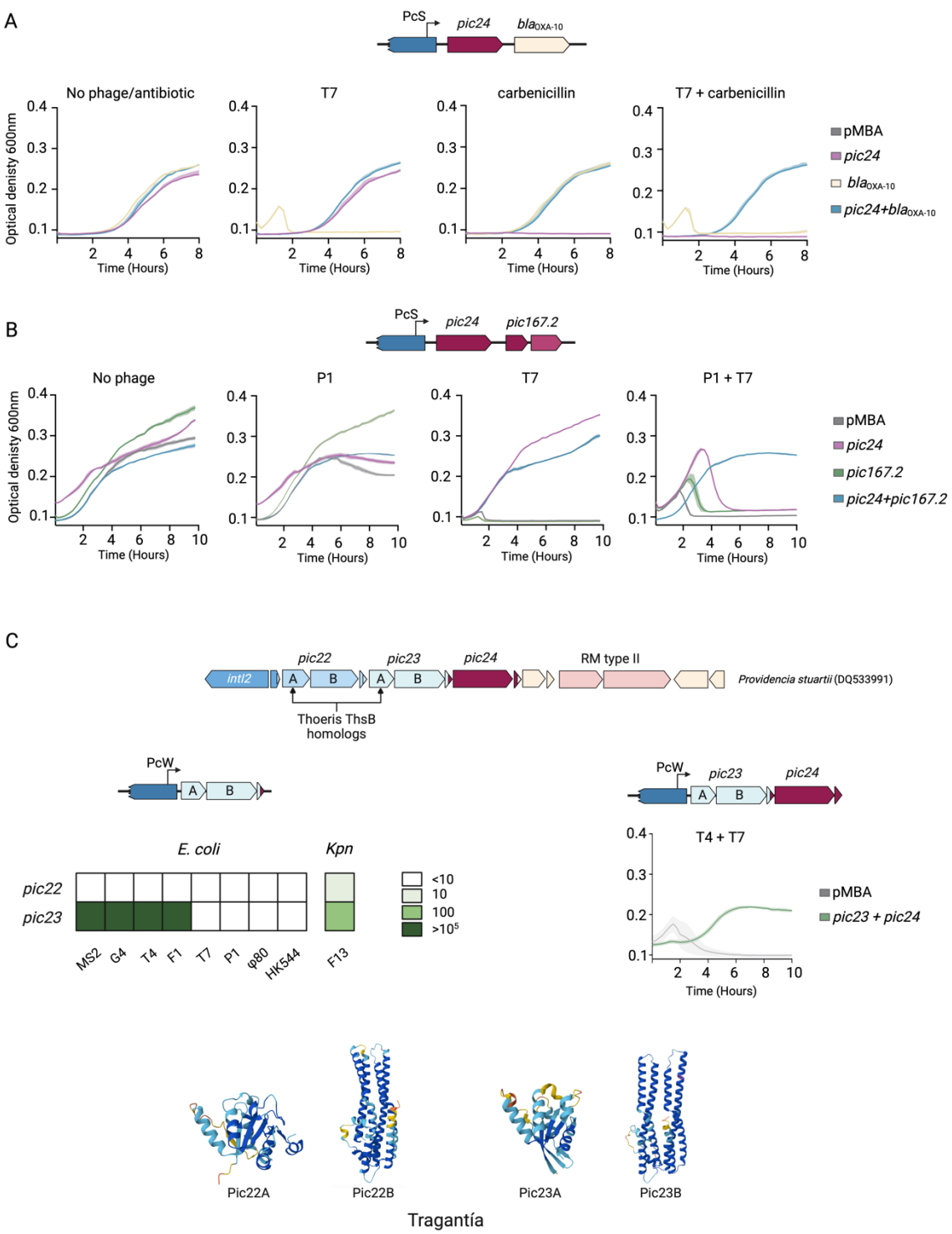

Figure 4. Additivity of Phage and Antibiotic Resistance Phenotypes in Multi-Cassette Arrays. Growth curves (OD_{600}) of *E. coli* strains containing **(A)** pMBA, *pic24* and *bla*$_{OXA-10}$ independently, and combined in an array in the absence of phage or antibiotic, and challenged with phage T7, carbenicillin, and a combination of both. The combined array confers resistance to phage and antibiotics simultaneously, and **(B)** pMBA, *pic24* and *pic167.2* independently, and combined in an array*;* either with no phage, or challenged with phage P1, phage T7, and a combination of both. (**C**) Genetic background of *pic24*. *pic22* and *pic23* contain homologs to TshB from Thoeris that confer resistance against phages from *E. coli* and *K. pneumoniae* (Kpn). *pic23* and *pic24* can confer multiphage resistance when in the same array. Growth curves are represented as the mean of three independent replicates. The standard error of the mean is represented as a lighter colour shade.

398 **PICs entail different fitness effects that vary across species.**

399 A major question in the field of phage defence is how these systems affect the fitness of
400 the host. This has important implications in the accumulation of such systems in genomes and
401 in their spread between species. Integrons are known to be low-cost platforms that can modulate
402 the expression of the genes in their cargo by changing their position in the array[21,53,54]. Yet the
403 cost of each cassette can be different, which is of importance in their dispersal through HGT.
404 To determine the cost of *pics*, we performed competition assays in both *E. coli* and *K.*
405 *pneumoniae* using flow cytometry (Figure 5). Our results showed a broad distribution of fitness
406 effects among PICs, ranging from large costs (ca. 40%) to virtually costless in both species. In
407 *E. coli, pic217*, *pic128* and *picN* seemed to have a mildly positive impact in fitness (up to 3%)
408 suggesting that acquisition of certain systems can be costless (Figure 5A). Interestingly, fitness
409 effects were not conserved between genetic backgrounds. For instance, *picWGS21* entailed a
410 small cost (ca. 7%) in *E. coli* but was very costly (ca. 30%) in *K. pneumoniae* (Figure 5B). Only
411 a few cassettes, like *picN* showed very similar cost in both species. The lack of cost of PICs in
412 certain genetic backgrounds, and the differences in fitness effects across backgrounds can be of
413 importance in the accumulation of cassettes and their preferential distribution of PICs among
414 species.

415 In the case of costly defence systems, a key advantage that integrons can provide,
416 compared to encoding them elsewhere, is that they can modulate their expression through the
417 distance to the Pc and the polar effects exerted by cassettes. Because the expression levels of
418 genes and their fitness cost generally correlate, we hypothesize that integrons can modulate the
419 fitness of PICs in the array. To test if the cost of a PIC can differ depending on the cassettes
420 upstream, we compared the cost entailed by *pic24* when located in first position of the array
421 (see above) with the cost it entails when encoded in third position (as it is found in the databases
422 (Figure 2A)). For this, we constructed an array (pArrayØ) containing two antibiotic resistance
423 cassettes, with strong polar effects (*aacA54* and *aacA8*)[54], and introduced *pic24* downstream,
424 as a third cassette (pArray-*pic24*). Competition experiments show that while *pic24* conferred a
425 fitness cost of 11% when located in first position, it had no significant cost when in third
426 position (Figure 5C). This was indeed due to the strong repression of its expression, since phage
427 infection experiments showed pArray-*pic24* did not protect against T7 infection. Hence, costly
428 PICs can be carried by mobile integrons at no cost to be later reshuffled into first position,
429 providing phage resistance (*adaptation-) on demand*[24] We also show that PICs exert polar
430 effects on downstream cassettes (Figure 5D), participating in the modulation of function and
431 cost that we have previously demonstrated for resistance genes[54].

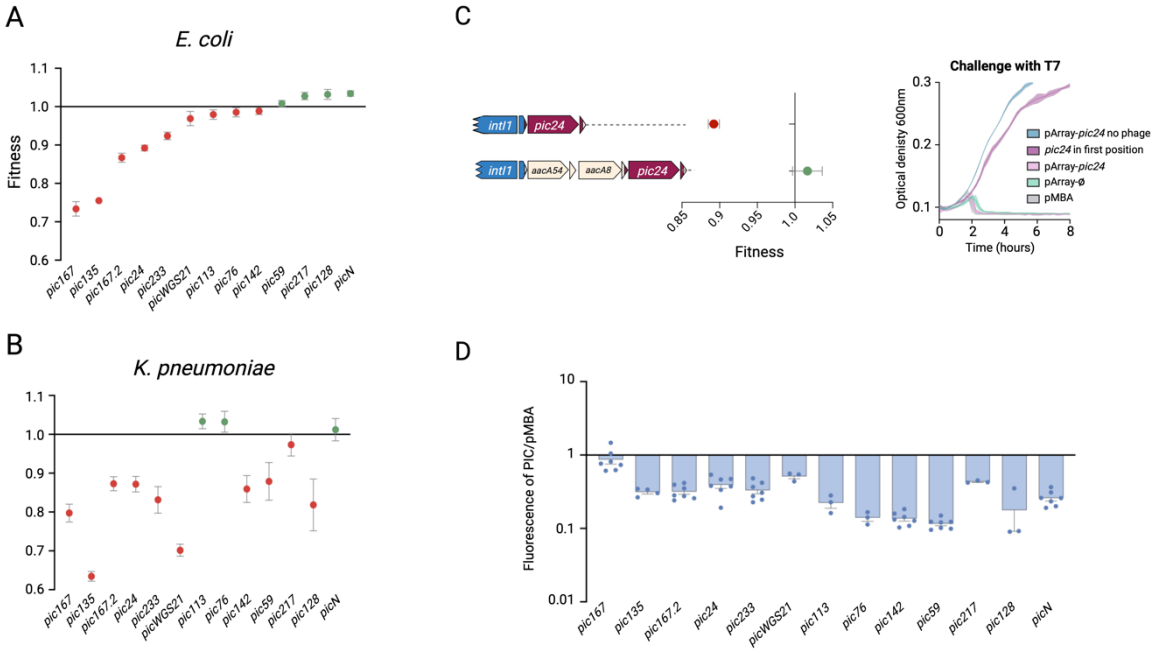

Figure 5. Fitness Effects of PICs. Fitness effects of PICs in **(A)** *E. coli* and **(B)** *K. pneumoniae*. Red circles represent fitness values below 1 (cost), while green circles indicate fitness values above 1 (gain). Fitness effects vary in sign and magnitude and are not conserved among genetic backgrounds. **(C)** Modulation of fitness cost and function by integron position. The graph shows the fitness effect of *pic24* in first position (competing pMBA vs pMBA-*pic24*) and third position (pArrayØ *vs.* pArray-*pic24*). The fitness cost imposed by the PIC is reduced in third position behind cassettes with strong polar effects. The cost is related to the function of the PIC since pArray-*pic24* does not confer resistance to T7. **(D)** Polar effects of PICs. All cassettes except *pic167* exert polar effects on downstream cassettes, limiting their expression. All assays have been performed at least three times. Error bars represent the standard error of the mean.

443 **DISCUSSION**

444 Phage therapy is an old approach with renewed interest in the light of the AMR
445 crisis[55,56]. It allows for personalized treatments against multidrug resistant bacteria, with
446 encouraging outcomes. Phage resistance is a rapidly evolving field of research. The constant
447 discovery of new resistance genes, often encoded in defence islands and prophages, reveals the
448 intense arms race between bacteria and their phages, and between mobile genetic elements. We
449 lack knowledge on how defence systems are recruited into these islands and on how frequently
450 they can move through HGT[13]. In contrast, mobile integrons are highly adaptable genetic
451 elements that have significantly contributed to the proliferation of multidrug resistance bringing
452 to our hospitals a plethora of resistance cassettes from the genomes of environmental bacteria.
453 Being shed to the environment at extremely high quantities (10^{23} per day)[57], mobile integrons
454 have established a strong communication route between the genomes of pathogenic and
455 environmental bacteria[58]. Hence, the rampant movement of mobile integrons among clinically
456 relevant bacteria ensures a high speed of dissemination of novel adaptive functions throughout
457 our hospitals. It is therefore critical for the future of phage therapy to understand the potential
458 role of integrons in phage defence. In this work we confirm that mobile integrons already
459 contain such systems.

460 We have successfully identified *pics* using bioinformatic tools and a phenotypic
461 screening with only T4 and T7 phages, and tested them against a panel of phages. As is the case
462 of most defence systems, *pics* displayed different specificities conferring narrow to broad
463 immunity in our assays. Nevertheless, because integrons can build arrays of cassettes, they can
464 combine phenotypes to confer multi-phage or phage-drug resistance, the same way they
465 currently confer multidrug resistance. In fact, *picN* is already found in an array with at least
466 three ARCs in a *P. aeruginosa* clinical isolate (Figure 2A). This, and other examples of
467 integrons containing *pic*s at different positions within the array, together with our results
468 showing that PICs can be carried at no cost, suggest that mobile integrons can become low-
469 cost, highly-mobile defence islands. An extreme case of this is shown by Darracq *et al*. in a
470 back-to-back paper in this issue, where they describe the presence of PICs in the Superintegron
471 of *Vibrio cholerae*. Indeed, in a recent work we have shown that the Superintegron is carried at
472 no measurable cost [59]. Additionally, their findings proves that chromosomal integrons are
473 virtually infinite repositories of PICs from where they can be recollected by mobile integrons.
474 Both Darracq *et al*. and us show that *pics* are functional in distant genetic backgrounds. In our
475 work, we show that this is the case in 3 of the 5 Gram negative species and strains of the
476 ESKAPEE group of highly resistant and dangerous pathogens: the kind of bacteria aimed by

477 phage therapy assays. This strongly suggests that the spread of PICs among them will be quick
478 if selective pressure with phages becomes commonplace. This has implications in what are
479 today considered as exploitable trade-offs in phage therapy. For instance, it is known that many
480 *K. pneumoniae* phages bind the bacterial capsule and that resistant clones can easily arise
481 through capsule loss, albeit at the cost of becoming non-virulent[60]. Also, in some cases
482 becoming resistant to phage infection through mutations comes at the cost of losing antibiotic
483 resistance[61,62]. The acquisition of plasmids containing integrons with *pics* can abrogate the
484 exploitability of such trade-offs, rendering virulence and antibiotic resistance perfectly
485 compatible with phage resistance.

486 The role of mobile integrons in phage resistance exemplifies the interplay between
487 mobile genetic elements. Indeed, many of the PICs described here target the conjugative pilus
488 of *E. coli* IJ1862. Hence, plasmids containing integrons can indirectly benefit from the activity
489 of PICs that protect their host. Mobile Integrons would alleviate the trade-off between acquiring
490 adaptive traits encoded in the plasmid and the susceptibility to a variety of phages. Another
491 aspect of this complex interplay is the potential link of *pic128* with plasmid stability. Contrarily
492 to the *ddmABC* system, *pic128* does not interact with p15A plasmid or with any natural plasmids
493 present in Kp5. This result highlights that not all Lamassu systems have the same activity
494 toward plasmids. The lack of anti-plasmid activity in Pic128AB might have a biological
495 meaning. Given that plasmid acquisition is an important source of antibiotic resistance, it is
496 possible that the lack of anti-plasmid activity of *pic128* has been selected for in an environment
497 with high antibiotic pressure. Additionally, the fact that certain pics could not be introduced in
498 *P. aeruginosa* (even under a weak Pc promoter) suggests that PICs can act as barriers to HGT.

499 Our work is not exempt of limitations. First, our screening -while successful in detecting
500 nine new genes- was based in the use of only T4 and T7. Given that some *pics* exhibit high
501 specificity against phages, it is likely that the number of *pic*s present in our collection of *gcus*
502 is underestimated. This could also apply to prophage-activation protection and plasmid stability
503 assays, if additional prophages and plasmids were tested. Additionally, algorithms to detect
504 defence systems are being constantly improved, so that detection of PICs in *gcus* will likely be
505 more prolific at the time this work is published.

506 This study shapes our perception of integrons. The presence of phage defence systems
507 and antibiotic resistance genes, proposes that integrons are protection elements against a large
508 breadth of environmental insults. This can guide the search for novel functions in the virtually
509 infinite reservoir of cassettes in nature. Our results have important implications in the field of
510 phage resistance, where mobile integrons provide extreme mobility at a very low and adjustable

fitness cost. Finding *pics* in Mobile integrons highlights the risk that phage resistance genes follow the same dissemination route as ARG in the past century. The field of phage therapy must be vigilant about the adaptive power of integrons since selective pressure will most likely make them -again- a key player in (phage-) resistance. If the importance of integrons in the evolution of phage resistance is neglected, it might come a day when phage hunting against clinical isolates becomes extremely difficult.

518 **MATERIAL AND METHODS**

519 **Strains and Phage collection**

520 *E. coli* DH5a and *P. aeruginosa* PAO1 are laboratory strains. *K. pneumoniae* KP5 is a clinical
521 isolate. *E. coli* 594[63], was kindly donated by José Penadés together with phages HK544 and
522 Φ80. Strains were grown at 37 °C in lysogeny broth (LB) or LB agar (1.5 %) (BD, France).
523 Zeocin was added at 100 µg/ml to maintain pMBA and pMBA-derived plasmids in *E. coli* and
524 *K. pneumoniae*. Tetracycline at 100 µg/ml was used to maintain pMBA plasmids in *P.*
525 *aeruginosa*. Liquid cultures were incubated in an Infors Multitron shaker at 200 rpm (Informs
526 HT, Swiss). Antibiotics were purchased from Sigma Aldrich (Merck, USA) except for zeocin
527 (InvivoGen, USA).

528 The coliphages included T4, T7, P1, MS2, G4, F1 which belong to the *Myoviridae*,
529 *Autographiviridae*, *Myoviridae*, *Fiersviridae*, *Microviridae* and *Inoviridae*, respectively. *E. coli*
530 phage MS2, F1, G4 and their host *E. coli* IJ1862[43] were kindly provided by from Prof. James J.
531 Bull (University of Texas). Phages T4, T7, and P1 were purchased from the DMSZ collection
532 (Leibniz, Germany). The *K. pneumoniae* phage, named F13, (found in effluents from a hospital)
533 was selected for its ability to lyse a clinical isolate called KP5, which produces the class D
534 carbapenemase OXA-48 and used as its host for this study. We computed the genomic data
535 obtained by Illumina technology with PHASTER to determined that F13 belongs to the
536 *Drexlerviridae* family. The *P. aeruginosa* PAO1 strain was used as a host for the Px4, Px5 and
537 Vs1 phages used in this study.

538 **Phage production**

539 We prepared phage solutions using previously published protocols[64]. Briefly, we grew host
540 bacteria in LB broth at 37ºC until they reached the exponential phase. At that point, we initiated
541 and monitored infection with the respective phage for 4 (for T7, T4, P1 phages) to 6 hours (for
542 MS2, G4, F1, HK544, and Φ80 phages). When we observed a decrease in optical density (OD),
543 we allowed the lysis process to continue for an additional hour. We then transferred the cultures
544 to polystyrene Falcon tubes for centrifugation and subsequent filtration using a 0.2 µm filter
545 (Sartorius, Spain) to collect the lysate containing the phage. Next, we titered the phage solutions
546 to determine the plaque-forming units (PFU). For plating, we mixed bacterial cultures (OD_{600}
547 ~1) with top agar medium and poured it onto agar dishes. After allowing it to dry for 30 minutes,
548 we spotted serial dilutions of the phages onto the agar plates and incubated them overnight at
549 37ºC[65].

550 ***In silico* analysis**

551 We generated the list of *gcus* using the INTEGRALL database (integrall.bio.ua.pt) and Integron
552 finder[33,45]. To determine if the *gcus* associated with known phage resistance defense systems,
553 we subjected the sequences of all *gcus* to a BLAST search against the two main defence system
554 databases: DefenseFinder[66] and PADLOC[35]. For *gcus* that showed a resistance phenotype but
555 remained unidentified by these platforms, we used an AlphaFold2 pipeline known as ColabFold
556 for prediction, followed by Foldseek to gain insights into the protein function of each *gcu*[67,68].
557 Additionally, we employed the Iterative Threading ASSEmbly Refinement (ITASSER)
558 platform to leverage complementary approaches for protein function prediction[69].

559 We carried out the sequencing of the *K. pneumoniae* isolate KP5 using a combination of
560 Illumina and Nanopore technologies, with SeqCoast (Portsmouth, USA) performing the
561 sequencing. We performed genome assembly using Unicycler software and conducted
562 subsequent analyses using the Center for Genomic Epidemiology platform. We determined the
563 resistome using the ResFinder web platform, identified the sequence type using MLST, and
564 characterized the plasmids using the PlasmidFinder web platform[70–72]. We assessed the
565 presence of prophages in the genome using the PHASTER web tool[73]. General DNA sequence
566 analysis was performed with Geneious and figures were created with BioRender.com.

567 **Cloning *gcu*s in pMBA**

568 All *gcus* were synthesized as double-stranded DNA by IDT ((Newark, USA), with an addition
569 of a 20 bp homology region corresponding to the targeted cloning site of pMBA located between
570 the *intI1* and *gfp* gene[32]. We performed the cloning process using the Gibson assembly method[74]
571 and selected clones on an LB agar plate supplemented with zeocin (50µg/mL). We cloned the
572 entire sequences of the *gcus*, including the open reading frame (ORF) and their *attC* region,
573 into the pMBA vector. Our in-house designed pMBA plasmid contains a p15A replication
574 origin, a zeocin resistance marker, and a truncated *intI1* gene followed by a *gfp* gene, acting as
575 a second integron cassette. We inserted the cloned *gcus* as the first cassette in the vector. To
576 ensure a relevant level of expression for each *gcu*, we selected a strong version of the Pc
577 promoter, PcS, located within the *intI1* gene, for our constructions. For the construction of
578 pArray-1 and pArray-2, we cloned at second position of the integron-like structure of pMBA
579 the $bla_{\text{OXA-10}}$ gene or the *pic167.2* instead of having the *gfp* gene, respectively. For the
580 construction of pArray-3, we cloned *pic23* and *pic 24* at first and second position, respectively,
581 of the integron-like structure present in pMBA under the control of a PcW promoter.

582 The construction of pArrayØ was accomplished using the Gibson assembly protocol, wherein
583 the *aacA54* and *aacA8* resistance gene cassettes were cloned into the pMBA-Δ*gfp* vector.

584 Subsequently, pArray-*pic24* was created by cloning the *pic24* gene into the third position of the
585 synthetic integron, downstream of the *aacA8* gene cassette.
586
587 For the cloning of *gcus* into *Pseudomonas aeruginosa* PAO1, we used a modified pMBA vector
588 (pBTZ). The p15A replication origin was replaced with the BBR1 origin to ensure replication
589 in both *E. coli* and *P. aeruginosa* species. Additionally, the strong PcS promoter was substituted
590 with its weaker version, PcW. Finally, a tetracycline resistance marker was introduced, as
591 *P. aeruginosa* exhibits low resistance to zeocin. The list of oligonucleotides used can be found
592 in Table S2.
593
594 **Growth curves and phage lysis monitoring**
595 We inoculated a single colony of a clone carrying a potential phage resistance gene into an
596 overnight culture of Luria Bertani (LB) broth at 37ºC. The next day, we adjusted the culture to
597 an optical density of 0.1 and transferred it to a 96-well plate containing LB broth supplemented
598 with zeocin (50 µg/mL). We then exposed the plate to different concentrations of phage to test
599 various multiplicities of infection (MOI). For all tested phages, we defined a high MOI
600 condition as an MOI of 1 and a low MOI condition as an MOI of 0,01. However, for phages T4
601 and T7, which exhibit high lytic activity, we set the high MOI condition to 0,01 and the low
602 MOI condition to 0,00001. We monitored growth curves using a Biotek HTX synergy plate
603 reader (Agilent , USA) at 600 nm over a 16-hour period. To assess the phage lysis level, we
604 calculated the area under the curve (AUC) for each growth condition, both with and without
605 phage as described previously[44]. The inhibition score for each sample was calculated using the
606 following formula:

607 $$Inhibition\ Score = \left(\frac{\Delta AUC}{\Delta AUC_{no\ phage}}\right) \times 100$$

608 where ΔAUC is the difference in AUC between the conditions with and without phage.
609 Specifically, $\Delta\mathrm{AUC} = \mathrm{AUC}_{no\ phage} - \mathrm{AUC}_{phage}$. We calculated the inhibition scores for both
610 high and low multiplicity of infection (MOI) conditions. These scores were then normalized by
611 comparing them to the inhibition scores obtained from the control samples, which used the
612 empty pMBA vector. The normalization was done by computing the ratio of the inhibition score
613 of the experimental sample to the inhibition score of the control: $Inhibition =$
614 $\left(\frac{Inhibition\ Score_{pic}}{Inhibition\ Score_{pMBA}}\right) \times 100$. By using the "inhibition score", we normalize the reduction of the
615 area under the curve relative to growth without the phage. This allows for comparison of the

616 relative effects regardless of initial growth differences between strains. The protective effect of
617 the PIC is shown as the inverse of the inhibition score.

618 **Prophage activation assay**

619 We chemically activate the lytic cycle of the prophages HK544 and Φ80 in E. coli 594::pMBA-
620 *pic* using mitomycin C at a concentration of 0,5 µg/mL. Briefly, we adjusted the culture to an
621 optical density of 0.1, and after 1h we induced prophage activation by adding mitomycin C.
622 Then, we quantitated the production of active phages after 6 hours of induction. To do so, we
623 centrifuged the culture we performed serial dilutions of the supernatant and spotted it on top
624 agar plate containing IJ-pMBA to evaluate the phage concentration[75].

625 **Phage-resistant clone screening**

626 To identify new phage defence integron cassettes, we employed both liquid and solid media
627 screening strategies. Initially, we cultured clones carrying various *gcus* overnight in LB broth
628 with zeocin (50 µg/mL). The following day, a 1 OD dilution of each culture (10 µL) was spotted
629 onto LB agar plates supplemented with zeocin. After 1 hour of incubation, we applied 7 µL of
630 phage T4 solution at a concentration of 10^9 PFU/mL to the bacterial spots. After 16-18 hours of
631 incubation, we selected the clones that exhibited growth despite phage presence for further
632 analysis. Additionally, we conducted a high-throughput screening in 96-well plates, challenging
633 the entire *gcu* collection with phages T7 and T4 under two different multiplicities of infection
634 (MOI) conditions, following the protocol described previously.

635 **Plasmid stability experiment**

636 We co-transformed *E. coli* IJ862 with both the empty pMBA plasmid carrying the p15A replicon
637 and the L-arabinose inducible pBAD plasmid carrying either the *pic128* or *ddmABC* defence
638 system. For five days, three replicates were put in culture in LB broth supplemented with
639 carbenicillin (100 µg/ml) and L-arabinose (0,1%). Daily, we transferred 50 µl of each culture
640 into fresh 5 ml LB broth and used another 50 µl to count GFP-expressing colonies on LB agar
641 plates supplemented with carbenicillin.

642 To assess the stability of the endogenous clinical plasmids in KP5 *K. pneumoniae* isolate, we
643 cultivated clones harbouring *pic128* in LB broth with zeocin (50 µg/ml) over five days. On days
644 1 and 5, we selected >120 colonies from LB zeocin agar plates and subcultured them onto
645 separate LB media containing either tetracycline (15 µg/ml), cefotaxime (50 µg/ml), or
646 ertapenem (30 µg/ml). This step aimed to detect any loss of resistance, which would suggest
647 the corresponding loss of one of the three natural plasmids.

648 ***attC* recombination experiments**

649 Recombination experiments were conducted as previously described[76]. Briefly, we cloned the
650 3' region of each *pic* using a pSW23T mobilizable plasmid containing a chloramphenicol
651 resistance marker into *E. coli* β2163 strain (*dapA*$^-$, *pir*$^+$) requiring diaminopimelic acid (DAP)
652 to grow. We used *E. coli* β2163 as donor strain for conjugation experiments using *E. coli* DH5α
653 strain carrying both a p3938 plasmid (Carb^R) containing an L-arabinose inducible *intI1* gene
654 and a p929 plasmid (Kana^R) containing an *attI* site as recipient. We performed conjugation
655 experiments onto LB agar supplemented with DAP and L-arabinose (0,2%) overnight. The next
656 day, after cell recover, we performed ten-folded dilutions onto LB agar supplemented with
657 carbenicillin (100 µg/ml) and glucose (1%) or with carbenicillin, glucose and chloramphenicol
658 (25 µg/ml) to select for the total population and recombinants, respectively.
659
660 **Fitness experiment**
661 To assess the fitness cost of each PIC, we performed *in vitro* competition assays following the
662 protocol described in[77] with some modifications. Briefly, we subcloned the panel of the 13 *PICs*
663 into a modified version of the pMBA vector, which includes a knock-out *gfp* gene (with a stop
664 codon instead of the start codon), along with an empty vector control. We then subjected this
665 new set of clones to a fitness competition experiment against the wild type pMBA vector
666 carrying the intact *gfp* gene. Briefly, we grew six replicates of each clone overnight at 37ºC in
667 a 96-well plate filled with LB broth supplemented with zeocin (50 µg/ml). The next day, we
668 mixed cells containing the target *gcu* in the pMBA-Δ*gfp* in a 1:1 volume ratio with the clone
669 carrying the pMBA-WT vector. We diluted these mixtures 1:20 in 96-well plates containing
670 NaCl 0,9%. This plate was further diluted 1:20 in a plate with NaCl and another with LB broth
671 supplemented with zeocin. The first plate was used to estimate the percentage of pMBA-WT
672 and pMBA-*pic*-Δ*gfp* cells in the mixture on day 1, using a Cytoflex S cytometer (Beckman
673 Coulter, USA). The second plate (with LB) was incubated overnight. The next day these
674 cultures were diluted 1:400 in NaCl to determine the proportion of strains in the mixture as
675 explained above. Following the formula described in[77], fitness cost was calculated as the
676 difference in ratios of GFP-fluorescence between day 1 and day 2 for each *PIC*.
677
678 **Quantitation of polar effects**
679 To determine the polar effects of cassettes, we measured the fluorescence of the Green
680 Fluorescent Protein (GFP) that acts as a second cassette in pMBA. At least three independent
681 colonies of each pMBA derived strain were inoculated in LB zeocin and incubated at 37ºC
682 overnight. Cultures were then diluted 1/400 in filtered saline solution to measure fluorescence

using a Cytoflex-S flow cytometer (Beckman Coulter). The 488 nm laser was used to detect GFP expression through 525/40 nm (FITC) band pass filter. 20,000 events were recorded per sample. Data were analysed using CytExpert software (v.2.4; Beckman Coulter).

ACKNOWLEDGEMENTS

We would like to thank Dr. José R. Penadés and Dr. James J. Bull for providing phages and strains, and Tamara Barcos for technical assistance. We thank André Carvalho for critical reading of the manuscript. NK is supported by funding from the European Union's Horizon 2020 research and innovation programme under the Marie Skłodowska-Curie grant agreement No 847635 for the ANARC research project (No 4230415). The work in the MBA laboratory is supported by the European Research Council (ERC) through a Starting Grant [803375]; Ministerio de Ciencia, Innovación y Universidades [BIO2017-85056-P; CNS2022-135857]; Ministerio de Ciencia e Innovación [PID2020-117499RB-100] and the EU HARISSA JPI-AMR program [PCI2021-122024-2A]; A.H. is supported by the PhD program at UCM. PB is supported by the Juan de la Cierva program (FJC 2020-043017-I). P.D-C. was supported by a Ramón y Cajal contract RYC2019-028015-I and the project PID2020-112835RA-I00, funded by MCIN/AEI/10.13039/501100011033, ESF Invest in your future; MG-Q is supported by the Subprograma Miguel Servet from the Ministerio de Ciencia e Innovación of Spain (CP19/00104), Instituto de Salud Carlos III (Plan Estatal de I+D+i 2017–2020), and co-funded by European Social Fund "Investing in your future". J.A.E. is supported by the Atracción de Talento Program of the Comunidad de Madrid [2016-T1/BIO-1105, 2020-5A/BIO-19726];

705 **REFERENCES**

706

707 1. Antimicrobial Resistance Collaborators. Global burden of bacterial antimicrobial
708 resistance in 2019: a systematic analysis. *Lancet* **399**, 629–655 (2022).
709 2. d'Herelle, F. Bacteriophage as a Treatment in Acute Medical and Surgical Infections.
710 *Bull N Y Acad Med* **7**, 329–48 (1931).
711 3. Hatfull, G. F., Dedrick, R. M. & Schooley, R. T. Phage Therapy for Antibiotic-Resistant
712 Bacterial Infections. *Annu Rev Med* **73**, 197–211 (2022).
713 4. Kortright, K. E., Chan, B. K., Koff, J. L. & Turner, P. E. Phage Therapy: A Renewed
714 Approach to Combat Antibiotic-Resistant Bacteria. *Cell Host Microbe* **25**, 219–232
715 (2019).
716 5. Labrie, S. J., Samson, J. E. & Moineau, S. Bacteriophage resistance mechanisms. *Nat*
717 *Rev Microbiol* **8**, 317–27 (2010).
718 6. Rostøl, J. T. & Marraffini, L. (Ph)ighting Phages: How Bacteria Resist Their Parasites.
719 *Cell Host Microbe* **25**, 184–194 (2019).
720 7. Bernheim, A. & Sorek, R. The pan-immune system of bacteria: antiviral defence as a
721 community resource. *Nat Rev Microbiol* **18**, 113–119 (2020).
722 8. Labrie, S. J., Samson, J. E. & Moineau, S. Bacteriophage resistance mechanisms. *Nat*
723 *Rev Microbiol* **8**, 317–27 (2010).
724 9. Millman, A. *et al.* An expanded arsenal of immune systems that protect bacteria from
725 phages. *Cell Host Microbe* **30**, 1556-1569.e5 (2022).
726 10. Vassallo, C. N., Doering, C. R., Littlehale, M. L., Teodoro, G. I. C. & Laub, M. T. A
727 functional selection reveals previously undetected anti-phage defence systems in the E.
728 coli pangenome. *Nat Microbiol* **7**, 1568–1579 (2022).
729 11. Dedrick, R. M. *et al.* Prophage-mediated defence against viral attack and viral counter-
730 defence. *Nat Microbiol* **2**, 16251 (2017).
731 12. Hochhauser, D., Millman, A. & Sorek, R. The defense island repertoire of the
732 Escherichia coli pan-genome. *PLoS Genet* **19**, e1010694 (2023).
733 13. Makarova, K. S., Wolf, Y. I., Snir, S. & Koonin, E. V. Defense Islands in Bacterial and
734 Archaeal Genomes and Prediction of Novel Defense Systems. *J Bacteriol* **193**, 6039–
735 6056 (2011).
736 14. Ghaly, T. M. *et al.* The Natural History of Integrons. *Microorganisms* **9**, (2021).
737 15. Labbate, M., Case, R. J. & Stokes, H. W. The Integron/Gene Cassette System: An
738 Active Player in Bacterial Adaptation. in 103–125 (2009). doi:10.1007/978-1-60327-
739 853-9_6.
740 16. Mazel, D. Integrons: Agents of bacterial evolution. *Nat Rev Microbiol* **4**, 608–620
741 (2006).
742 17. Recchia, G. D. & Hall, R. M. Gene cassettes: A new class of mobile element.
743 *Microbiology (N Y)* **141**, 3015–3027 (1995).
744 18. Partridge, S. R. *et al.* Definition of the attI1 site of class 1 integrons. *Microbiology (N*
745 *Y)* **146**, 2855–2864 (2000).
746 19. Collis, C. M. & Hall, R. M. Expression of antibiotic resistance genes in the integrated
747 cassettes of integrons. *Antimicrob Agents Chemother* **39**, 155–162 (1995).
748 20. Barraud, O. & Ploy, M. C. Diversity of class 1 integron gene cassette rearrangements
749 selected under antibiotic pressure. *J Bacteriol* **197**, 2171–2178 (2015).

21. Souque, C., Escudero, J. A. & Maclean, R. C. Integron activity accelerates the evolution of antibiotic resistance. *Elife* **10**, 1–47 (2021).
22. Carvalho, A. *et al.* The expression of integron arrays is shaped by the translation rate of cassettes. doi:10.1101/2024.03.26.586746.
23. Guerin, É. *et al.* The SOS Response Controls Integron Recombination. *Science (1979)* **324**, 1034–1034 (2009).
24. Antonio Escudero, J., Loot, C., Nivina, A. & Mazel, D. The Integron: Adaptation On Demand. *Mobile DNA III* 139–161 (2015) doi:10.1128/9781555819217.ch6.
25. Partridge, S. R., Kwong, S. M., Firth, N. & Jensen, S. O. Mobile Genetic Elements Associated with Antimicrobial Resistance. *Clin Microbiol Rev* **31**, (2018).
26. Stokes, H. W. & Hall, R. M. A novel family of potentially mobile DNA elements encoding site-specific gene-integration functions: integrons. *Mol Microbiol* **3**, 1669–1683 (1989).
27. Domingues, S., da Silva, G. J. & Nielsen, K. M. Integrons: Vehicles and pathways for horizontal dissemination in bacteria. *Mob Genet Elements* **2**, 211–223 (2012).
28. Mitsuhashi, S., Harada, K., Hashimoto, H. & Egawa, R. On the drug-resistance of enteric bacteria. 4. Drug-resistance of Shigella prevalent in Japan. *Jpn J Exp Med* **31**, 47–52 (1961).
29. Kaushik, M., Kumar, S., Kapoor, R. K., Virdi, J. S. & Gulati, P. Integrons in Enterobacteriaceae : diversity, distribution and epidemiology. *Int J Antimicrob Agents* **51**, 167–176 (2018).
30. Hipólito, A., García-Pastor, L., Vergara, E., Jové, T. & Escudero, J. A. Profile and resistance levels of 136 integron resistance genes. *npj Antimicrobials and Resistance* **1**, 13 (2023).
31. Partridge, S. R., Tsafnat, G., Coiera, E. & Iredell, J. R. Gene cassettes and cassette arrays in mobile resistance integrons. *FEMS Microbiol Rev* **33**, 757–784 (2009).
32. Hipólito, A. *et al.* The expression of aminoglycoside resistance genes in integron cassettes is not controlled by riboswitches. *Nucleic Acids Res* (2022) doi:10.1093/nar/gkac662.
33. Moura, A. *et al.* INTEGRALL: A database and search engine for integrons, integrases and gene cassettes. *Bioinformatics* **25**, 1096–1098 (2009).
34. Tesson, F. *et al.* Systematic and quantitative view of the antiviral arsenal of prokaryotes. *Nat Commun* **13**, 2561 (2022).
35. Payne, L. J. *et al.* PADLOC: a web server for the identification of antiviral defence systems in microbial genomes. *Nucleic Acids Res* **50**, W541–W550 (2022).
36. Payne, L. J. *et al.* PADLOC: a web server for the identification of antiviral defence systems in microbial genomes. *Nucleic Acids Res* **50**, W541–W550 (2022).
37. Rousset, F. *et al.* Phages and their satellites encode hotspots of antiviral systems. *Cell Host Microbe* **30**, 740-753.e5 (2022).
38. Jaskólska, M., Adams, D. W. & Blokesch, M. Two defence systems eliminate plasmids from seventh pandemic Vibrio cholerae. *Nature* **604**, 323–329 (2022).
39. Duncan-Lowey, B. & Kranzusch, P. J. CBASS phage defense and evolution of antiviral nucleotide signaling. *Curr Opin Immunol* **74**, 156–163 (2022).
40. Haaber, J., Moineau, S., Fortier, L.-C. & Hammer, K. AbiV, a novel antiphage abortive infection mechanism on the chromosome of Lactococcus lactis subsp. cremoris MG1363. *Appl Environ Microbiol* **74**, 6528–37 (2008).

41. Matelska, D., Steczkiewicz, K. & Ginalski, K. Comprehensive classification of the PIN domain-like superfamily. *Nucleic Acids Res* **45**, 6995–7020 (2017).
42. Boyd, C. D. *et al.* Structural Features of the Pseudomonas fluorescens Biofilm Adhesin LapA Required for LapG-Dependent Cleavage, Biofilm Formation, and Cell Surface Localization. *J Bacteriol* **196**, 2775–2788 (2014).
43. Bull, J. J., Badgett, M. R., Springman, R. & Molineux, I. J. Genome properties and the limits of adaptation in bacteriophages. *Evolution (N Y)* **58**, 692 (2004).
44. Quinones-Olvera, N. *et al.* Diverse and abundant phages exploit conjugative plasmids. *Nat Commun* **15**, (2024).
45. Néron, B. *et al.* IntegronFinder 2.0: Identification and Analysis of Integrons across Bacteria, with a Focus on Antibiotic Resistance in Klebsiella. *Microorganisms* **10**, (2022).
46. Bouvier, M., Demarre, G. & Mazel, D. Integron cassette insertion: A recombination process involving a folded single strand substrate. *EMBO Journal* **24**, 4356–4367 (2005).
47. Loot, C., Ducos-Galand, M., Escudero, J. A., Bouvier, M. & Mazel, D. Replicative resolution of integron cassette insertion. *Nucleic Acids Res* **40**, 8361–8370 (2012).
48. Bouvier, M., Ducos-Galand, M., Loot, C., Bikard, D. & Mazel, D. Structural features of single-stranded integron cassette attC sites and their role in strand selection. *PLoS Genet* **5**, (2009).
49. Nivina, A., Escudero, J. A., Vit, C., Mazel, D. & Loot, C. Efficiency of integron cassette insertion in correct orientation is ensured by the interplay of the three unpaired features of attC recombination sites. *Nucleic Acids Res* **44**, 7792–7803 (2016).
50. MacDonald, D., Demarre, G., Bouvier, M., Mazel, D. & Gopaul, D. N. Structural basis for broad DNA-specificity in integron recombination. *Nature* **440**, 1157–1162 (2006).
51. Blanco, P. *et al.* Identification of Promoter Activity in Gene-Less Cassettes from Vibrionaceae Superintegrons. *Nucleic Acids Research. In press* (2023) doi:10.1101/2023.11.21.568050.
52. Barlow, R. S. & Gobius, K. S. Diverse class 2 integrons in bacteria from beef cattle sources. *Journal of Antimicrobial Chemotherapy* **58**, 1133–1138 (2006).
53. Lacotte, Y., Ploy, M.-C. & Raherison, S. Class 1 integrons are low-cost structures in Escherichia coli. *ISME J* **11**, 1535–1544 (2017).
54. Carvalho, A. *et al.* The expression of integron arrays is shaped by the translation rate of cassettes. 2 3 ORCID. doi:10.1101/2024.03.26.586746.
55. Corbellino, M. *et al.* Eradication of a Multidrug-Resistant, Carbapenemase-Producing Klebsiella pneumoniae Isolate Following Oral and Intra-rectal Therapy With a Custom Made, Lytic Bacteriophage Preparation. *Clinical Infectious Diseases* **70**, 1998–2001 (2020).
56. Pirnay, J.-P. *et al.* Personalized bacteriophage therapy outcomes for 100 consecutive cases: a multicentre, multinational, retrospective observational study. *Nat Microbiol* **9**, 1434–1453 (2024).
57. Zhu, Y.-G. *et al.* Microbial mass movements. *Science (1979)* **357**, 1099–1100 (2017).
58. Gillings, M. *et al.* The evolution of class 1 integrons and the rise of antibiotic resistance. *J Bacteriol* **190**, 5095–5100 (2008).
59. Blanco, P. *et al.* Chromosomal Integrons are Genetically and Functionally Isolated Units of Genomes 2 3. doi:10.1101/2023.11.17.567518.

60. Song, L. *et al.* Phage Selective Pressure Reduces Virulence of Hypervirulent Klebsiella pneumoniae Through Mutation of the wzc Gene. *Front Microbiol* **12**, (2021).
61. Fujiki, J., Nakamura, K., Nakamura, T. & Iwano, H. Fitness Trade-Offs between Phage and Antibiotic Sensitivity in Phage-Resistant Variants: Molecular Action and Insights into Clinical Applications for Phage Therapy. *Int J Mol Sci* **24**, 15628 (2023).
62. Chan, B. K. *et al.* Phage selection restores antibiotic sensitivity in MDR Pseudomonas aeruginosa. *Sci Rep* **6**, 26717 (2016).
63. Alqurainy, N. *et al.* A widespread family of phage-inducible chromosomal islands only steals bacteriophage tails to spread in nature. *Cell Host Microbe* **31**, 69-82.e5 (2023).
64. Bonilla, N. *et al.* Phage on tap-a quick and efficient protocol for the preparation of bacteriophage laboratory stocks. *PeerJ* **4**, e2261 (2016).
65. Ács, N., Gambino, M. & Brøndsted, L. Bacteriophage Enumeration and Detection Methods. *Front Microbiol* **11**, 594868 (2020).
66. Tesson, F. *et al.* Systematic and quantitative view of the antiviral arsenal of prokaryotes. *Nat Commun* **13**, 2561 (2022).
67. van Kempen, M. *et al.* Fast and accurate protein structure search with Foldseek. *Nat Biotechnol* (2023) doi:10.1038/s41587-023-01773-0.
68. Mirdita, M. *et al.* ColabFold: making protein folding accessible to all. *Nat Methods* **19**, 679–682 (2022).
69. Yang, J. & Zhang, Y. Protein Structure and Function Prediction Using I-TASSER. *Curr Protoc Bioinformatics* **52**, (2015).
70. Bortolaia, V. *et al.* ResFinder 4.0 for predictions of phenotypes from genotypes. *Journal of Antimicrobial Chemotherapy* **75**, 3491–3500 (2020).
71. Carattoli, A. *et al. In Silico* Detection and Typing of Plasmids using PlasmidFinder and Plasmid Multilocus Sequence Typing. *Antimicrob Agents Chemother* **58**, 3895–3903 (2014).
72. Larsen, M. V. *et al.* Multilocus Sequence Typing of Total-Genome-Sequenced Bacteria. *J Clin Microbiol* **50**, 1355–1361 (2012).
73. Arndt, D. *et al.* PHASTER: a better, faster version of the PHAST phage search tool. *Nucleic Acids Res* **44**, W16–W21 (2016).
74. Avilan, L. Assembling Multiple Fragments: The Gibson Assembly. *Methods Mol Biol* **2633**, 45–53 (2023).
75. Ibarra-Chávez, R., Reboud, J., Penadés, J. R. & Cooper, J. M. Phage-Inducible Chromosomal Islands as a Diagnostic Platform to Capture and Detect Bacterial Pathogens. *Adv Sci (Weinh)* **10**, e2301643 (2023).
76. Biskri, L., Bouvier, M., Guérout, A. M., Boisnard, S. & Mazel, D. Comparative study of class 1 integron and Vibrio cholerae superintegron integrase activities. *J Bacteriol* **187**, 1740–1750 (2005).
77. DelaFuente, J., Rodriguez-Beltran, J. & San Millan, A. Methods to Study Fitness and Compensatory Adaptation in Plasmid-Carrying Bacteria. *Methods in Molecular Biology* **2075**, 371–382 (2020).